IEEE Access
Multidisciplinary | Rapid Review | Open Access Journal

Received April 16, 2019, accepted May 12, 2019, date of publication May 22, 2019, date of current version June 5, 2019.

Digital Object Identifier 10.1109/ACCESS.2019.2918218

Echo Signal Extraction Based on Improved Singular Spectrum Analysis and Compressed Sensing in Wavelet Domain

XIAOBIN XU[1,2], MIN ZHANG[1,2], MINZHOU LUO[1,2], JIAN YANG[3], QINYANG QU[1,2], ZHIYING TAN[1,2], AND HAO YANG[1,2]

[1]College of Mechanical and Electrical Engineering, Hohai University, Changzhou 213022, China
[2]Jiangsu Key Laboratory of Special Robot Technology, Hohai University, Changzhou 213022, China
[3]College of Mechanical Engineering, Yangzhou University, Yangzhou 225127, China

Corresponding author: Xiaobin Xu (xxbtc@hhu.edu.cn)

This work was supported in part by the National Natural Science Foundation of China under Grant 51805146, in part by the Changzhou Sci&Tech Program under Grant CJ20180047, and in part by the Fundamental Research Funds for the Central Universities under Grant 2017B07814.

ABSTRACT A novel framework of signal extraction is proposed based on improved singular spectrum analysis (SSA) and compressed sensing (CS) for laser radar. The improved signal selection method, which locates a cut-off point on the singular spectrum curve, is fused into the SSA to reduce the noise. Afterward, the CS in the wavelet domain is employed to acquire the observation vector, and the improved reconstruction algorithm with a hard threshold denoising method reduces the noise furthermore. The simulations and experiments are performed to verify the superiority of the proposed algorithm compared with other algorithms. The proposed algorithm can enhance a signal-to-noise ratio while reducing the distortion of the received signal.

INDEX TERMS Laser radar, signal denoising, singular spectrum analysis, compressed sensing, wavelet transforms.

I. INTRODUCTION

Recently, with the advantages of high precision and high resolution, laser radar is widely used in various fields, such as unmanned vehicles [1]–[3], remote sensing [4], [5], mobile robots [6], [7], etc. Laser radars are divided into two categories: direct detection laser radars and coherent laser radars, where direct detection laser radar measures the round-trip time of laser pulse and achieves the distance between the target and itself by using time-of-flight method. It has been noted that ranging distribution and precision of laser radar are directly affected by signal-to-noise ratio (SNR) [8]. Previous works demonstrated that ranging precision declined with the decreasing of SNR [9]. Especially in low SNR, the received signal buried in noise is not detected and recognized using classical analog methods such as peak detection (PD), leading edge detection (LED) and constant fraction discriminator (CFD) [10], [11]. Thus, it is crucial to extract received signals through denoising methods.

The associate editor coordinating the review of this manuscript and approving it for publication was Chenhao Qi.

Fourier transform (FT) [12], as a classical signal analysis method, is not suitable for non-stationary noisy received signal. In order to reduce noise of non-stationary signal, there are a number of researches available proposing with Time-frequency analysis methods, such as short time Fourier transform (STFT) [13], discrete wavelet transform (DWT) [14]–[16], empirical mode decomposition (EMD) [17], [18], Singular spectrum analysis (SSA) [19], etc. Although STFT overcomes the deficiency of FT, it is difficult of finding proper length of window function for achieving ideal denoised effect. The well-known wavelet threshold denoising method derived from DWT has been applied in lidar [20], imaging process [21] and gear fault diagnosis [22], etc. The most critical components of wavelet denoising algorithms are threshold function, wavelet base and decomposition level. Previous researches have mainly focused on threshold functions. Donohon proposed the hard and soft threshold function to reduce signal noise [23]. Zhou and Li employed soft threshold function to extract lidar echo signals [15], [20]. However, hard function will cause additional oscillation and discontinuity point of signal. Since soft

threshold function ameliorates signal quality, the similarity between reconstructed signal and original signal is reduced. Hence, some scholars put forward other continuous derivable threshold functions such as the power function [24], [25], semi-soft function [21] and sine function [26]. Nevertheless, if the threshold function and threshold are not appropriate for specific signal, the quality of the denoised result is not guaranteed. Moreover, wavelet denoising algorithm cannot achieve high temporal and frequency resolution simultaneously. EMD decomposes the signal adaptively and obtains the complete signal component. But mode mixing and end effect will affect the precision of signal denoising and extraction [27], [28].

SSA is a powerful method for studying nonlinear time series and signal processing. It constructs the trajectory matrix according to the observed time series. The signals representing different components are extracted combined with decomposition and reconstruction of trajectory matrix. If signal and noise are regarded as two components of original time series, the boundary point of two groups of signal is especially significant. Traditional selection methods of boundary point are derived from singular value difference spectrum [29], singular value curvature spectrum [30], and singular entropy increment [31]. Since there is no obvious distinction between curves depicted by singular value and singular entropy increment except the amplitude. Compared with singular value curvature spectrum, the difference spectrum method is not adequate to distinguish the cut-off point of singular value due to the sparse feature of difference spectrum curve. Thus, it is more convenient by using singular value curvature spectrum. However, peak selection method in Ref [30] is not always efficient for echo signal. Therefore, a novel selection criterion should be updated. What's more, this bound point is not completely accurate, and another denoising method should be utilized.

Compared with above methods, compressed sensing (CS) theory, firstly put forward by Donoho *et al.* [32], not only reduces the noise in reconstruction, but also avoids the threshold selection of DWT and EMD methods. Based on CS theory, clean signal is represented as a spot of none-zero elements, which are so-called K-sparsity in certain orthogonal space. Combing with observation matrix and sparsity, the original signal is recovered through specific algorithms, which are primarily separated into two parts: convex optimization algorithms and greedy algorithms [33]. In summary, there are three problems of CS method: sparse decomposition, recovery algorithm and K-sparsity. (1) In the aspect of CS decomposition, both Chen and Qu adopted DCT and FFT to decompose the noisy signal respectively [34], [35]. However, it is mostly not reasonable to use DCT and FFT because of the Gaussian characteristic of the received laser signal. Despite Zhao exploited detail coefficients to reduce the noise [36], the recovery signal in every decomposition level is composed of at least one element. Thus, the noise contained in the detail coefficients is not completely removed to all intents and purposes. (2) In addition, compared with greedy algorithms, it is tough to adopt convex optimization algorithm because of the limitations of complexity and computation cost. Contrarily, matching pursuit (MP) and orthogonal matching pursuit (OMP), as representative greedy algorithms, are easy to realize signal recovery [37]. Furthermore, regularized orthogonal matching pursuit (ROMP), compressive sampling matching pursuit (CoSaMP), subspace pursuit (SP) algorithms and generalized orthogonal matching pursuit (GOMP), as modified OMP algorithms, were proposed and used to accelerate convergence on each iteration by exploiting multiple atoms [38]–[41]. (3) Nevertheless, algorithms above require prior knowledge about the sparsity that is not acquired for natural signal. Hence, stagewise orthogonal matching pursuit (StOMP) and stagewise weak orthogonal matching pursuit (SWOMP) were proposed to make up for shortcomings and adaptively reconstruct signal without knowing sparsity in advance [42], [43]. However, due to existence of wrong atoms, accurate recovery of approximately sparse signal is not guaranteed as well. Moreover, the CS reconstruction is not efficient, once SNR is less than certain threshold.

In order to solve above problems, we proposed improved SSA to realize pre-denoising. Afterwards, the CS theory in wavelet domain is employed to decompose the received laser signal. Both of approximate coefficients and detail coefficients are conducted to recovery signal. The improved GOMP (IGOMP) is proposed to bring about signal reconstruction and enhance denoising effect.

The remainder of the paper is organized as follows. In Section 2, the model of noisy signal is given combing laser radar system. In Section 3, two-stage denoising framework is proposed. The singular value selection method is added to SSA algorithm to reduce the noise. Afterwards, the CS in wavelet domain is employed to acquire the observation vector, and the improved GOMP reconstruction algorithm with hard threshold denoising method enhances SNR furthermore. In Section 4, SNR and peak time error are conducted to evaluate denoised effect with different algorithms. In Section 5, the experiments are carried out and verified the superiority of proposed algorithm for noisy signal. Finally, some conclusions are given.

II. PRINCIPLE OF LASER RADAR

The laser radar consists of laser emitted system, laser receiving system and signal processing system. The working diagram of laser radar is shown in Fig.1. The pulse laser beam, generated by laser diode and laser emitting circuit, is collimated into the narrow pulse beam with collimated lens. Afterwards, the narrow beam propagates in atmosphere through a 45-degree reflector. Whilst the scattered light reflected from the target irradiates on the avalanche photodiode (APD) through filter and focusing lens, the pulse laser light is converted into the pulse current signal, which is amplified with laser receiving circuit. Thus, the distance between target and laser radar is calculated.

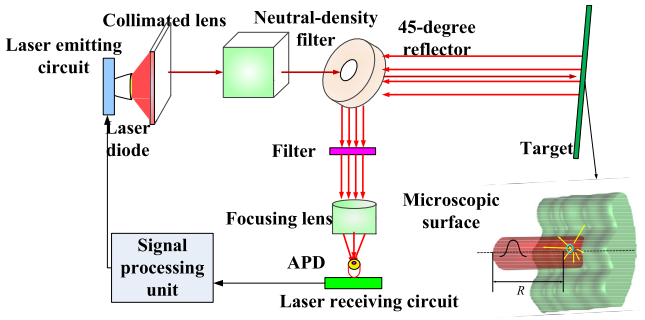

FIGURE 1. The working diagram of laser radar.

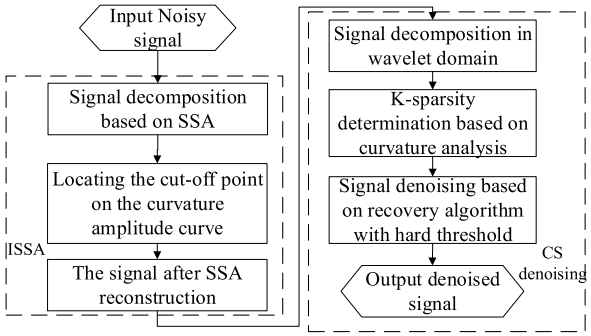

FIGURE 2. Flow chart of two-stage denoising framework.

Based on literature [8], the voltage of receiving signal is regarded as linear superposition of two Gaussian functions, and then we can write it as:

$$V(t) = A_1 e^{-(t-t_1)^2/2\tau_1^2} + A_2 e^{-(t-t_2)^2/2\tau_2^2} + A_3 \tag{1}$$

where A_1 and A_2 are the amplitudes of two Gaussian functions, respectively, A_3 is the direct current voltage, t_1 and t_2 are the peak time of two Gaussian functions, respectively, and τ_1 and τ_2 are pulse widths, respectively.

The noisy signal is represented as:

$$V_{sn}(t) = V(t) + V_n(t) \tag{2}$$

where $V_n(t)$ is noise signal.

The probability distribution of noise signal, described as Gaussian distribution, is written as:

$$p\left(V_n(t)\right) = \frac{1}{\sqrt{2\pi}\,\overline{V}_n} \exp\left(-\frac{V_n^2(t)}{2\overline{V}_n^2}\right) \tag{3}$$

where $\overline{V}_n$ is equivalent root mean square (RMS) noise voltage.

III. TWO-STAGE DENOISING ALGORITHM

Two-stage denoising framework is composed of improved singular spectrum analysis and CS denoising in wavelet domain. Fig. 2 displays flow chart of denoising framework. In pre-denoising stage, the cut-off selection method is proposed. In CS denoising stage, the signal is decomposed in wavelet domain, and then adaptive K-sparsity determination method is put forward by using curvature analysis. Finally, the improved recovery algorithm with hard threshold method is employed to enhance the probability of signal reconstruction.

A. IMPROVED SINGULAR SPECTRUM ANALYSIS

Classical SSA method is divided into four steps: data embedding, singular value decomposition (SVD), grouping and diagonal averaging [19].

1) STEP1: DATA EMBEDDING

The laser noisy signal is: $\boldsymbol{s}_N = \{c_i\}\ i = 1, \cdots, N$. The Hankel matrix is constructed using data embedding method. Assume that the row number of data embedding is n, and the column number is $N - n + 1$. The Hankel matrix is represented as:

$$\boldsymbol{H} = \begin{bmatrix} c_1 & c_2 & \cdots & c_n \\ c_2 & c_3 & \cdots & c_{n+1} \\ \vdots & \vdots & \vdots & \vdots \\ c_{N-n+1} & c_{N-n+2} & \cdots & c_N \end{bmatrix} \tag{4}$$

2) STEP2: SINGULAR VALUE DECOMPOSITION

After data embedding, the matrix $\boldsymbol{H}$ with SVD is rewritten as:

$$\boldsymbol{H} = \boldsymbol{U}\boldsymbol{\Sigma}\boldsymbol{V}^{\mathrm{T}} \tag{5}$$

where $\boldsymbol{U}$ and $\boldsymbol{V}$ are orthogonal matrices, and $\boldsymbol{\Sigma}$ is diagonal matrix, which consists of singular values. Vector groups $\{\boldsymbol{u}_i\}$ of $\boldsymbol{U}$ are the orthonormal normalized eigenvectors of matrix $\boldsymbol{H}\boldsymbol{H}^{\mathrm{T}}$. Vector groups $\{\boldsymbol{v}_i\}$ of $\boldsymbol{V}$ are the orthonormal normalized eigenvectors ofmatrix $\boldsymbol{H}^{\mathrm{T}}\boldsymbol{H}$.

Considering the $l = \mathrm{rank}(H)$, the Hankel matrix can be expressed as:

$$\boldsymbol{H} = \sum_{i=1}^{l} \boldsymbol{H}_i = \sum_{i=1}^{l} \boldsymbol{u}_i \sigma_i \boldsymbol{v}_i^{\mathrm{T}} \tag{6}$$

where the singular values are listed in descending order: $\sigma_1 \geq \sigma_2 \geq \cdots \geq \sigma_l \geq 0$.

3) STEP3: GROUPING

Based on the grouping principle, the set of indices $\{1, \ldots, l\}$ are partitioned into I_G irrelevant subsets $I_1, I_2, \ldots, I_G$. Let $I_i = \{i_1, \ldots, i_p\}$ be the ith subset. The subset matrix and Hankel matrix can be expressed as

$$\boldsymbol{H}_{I_i} = \boldsymbol{H}_{i_1} + \boldsymbol{H}_{i_2} + \cdots + \boldsymbol{H}_{i_P} \tag{7}$$

$$\boldsymbol{H} = \boldsymbol{H}_{I_1} + \boldsymbol{H}_{I_2} + \cdots + \boldsymbol{H}_{I_G} \tag{8}$$

4) STEP4: DIAGONAL AVERAGING

By applying diagonal averaging method to $\boldsymbol{H}_{I_i} = (a_{ij})_{(N-n+1)\times n}$, the zth element of signal reconstruction

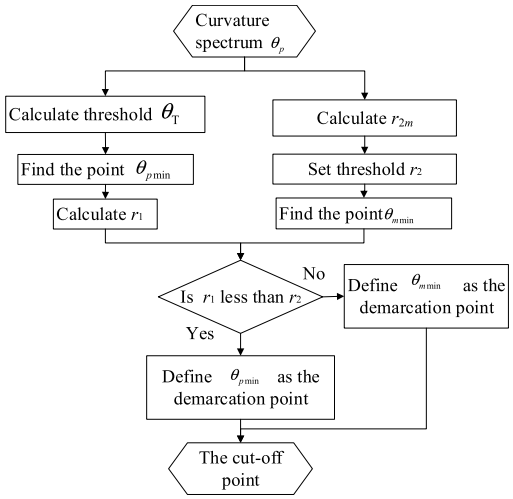

FIGURE 3. The flow chart of proposed method.

components $\boldsymbol{RC}_{I_i}$ is given by:

$$\boldsymbol{RC}_z = \begin{cases} \dfrac{1}{z}\displaystyle\sum_{j=1}^{z} a_{j,z-j+1} & 1 \le z \le N-n+1 \\ \dfrac{1}{N-n+1}\displaystyle\sum_{j=1}^{N-n+1} a_{j,z-j+1} & N-n+1 \le z \le n \\ \dfrac{1}{N-z+1}\displaystyle\sum_{j=z-n+1}^{N-n+1} a_{j,z-j+1} & n \le z \le N \end{cases} \tag{9}$$

In fact, the original signal is recombined as:

$$\boldsymbol{s} = \sum_{i=1}^{M} \boldsymbol{RC}_{I_i} \tag{10}$$

According to reference [29], singular values of $\boldsymbol{\Sigma}$ are nonzero for the noisy signal. The characteristic of singular values is: $\sigma_1 > \sigma_2 > \cdots > \sigma_k \gg \sigma_{k+1} > \cdots > \sigma_l$. Let G be 2, and determine k using specific method. We can construct the denoised signal by Eqs. (9) and (10). In this paper, we adopt singular value curvature spectrum. We select k value traditionally according to the peak location. There is no evidence showing that the peak location is optimal especially in case of multi peak curve. Moreover, we reduce partial noise to ensure the efficiency of denoising method based on CS theory using the SSA method. In order to choose a better k value, we relax the requirements and put forward the two selection rules. The flow chart of proposed method is shown in Fig. 3.

The procedure is outlined as follows:

Step1: Find local peak points of curvature amplitude curve $\theta_p, p = 1, 2, 3\cdots$.

Step2: Define threshold θ_T as $\text{mean}(\sigma_k) + q_1 \cdot \text{std}(\sigma_k)$, and q_1 is adjustable factor. Let the minimum curvature point $\theta_{p\min}$ be greater than the threshold θ_T. The ratio of energy from start point to $\theta_{p\min}$ to noisy signal energy is detonated as r_1.

Step3: Define the ratio of energy from start point to $\theta_m, m = 1, 2, 3\cdots$ to noisy signal energy as r_{2m}. Set threshold r_2. Let the minimum curvature point $\theta_{m\min}$ be greater than the threshold r_2.

Step4: If $r_1 > r_2$, the location of $\theta_{p\min}$ is defined as the cut-off point. Otherwise, define location of $\theta_{m\min}$ as cut-off point.

Step5: The cut-off point is determined and output.

In order to estimate the parameter r_2, the noisy signal sequence, whose absolute value is three times larger than the estimated noise, is selected. The parameter r_2 is calculated by these selected signal parts.

Since we reduce the partial noise, the received voltage signal still contains residue noise. It is necessary to use denoised method based on CS theory.

B. COMPRESSED SENSING IN WAVELET DOMAIN

The clean signal $\boldsymbol{x}$, denoted as $N \times 1$ column vector of space R^N, can be expressed with the linear combination of the base vectors $\{\boldsymbol{\psi_i} | i = 1, 2, \ldots N\}$. Thus, signal $\boldsymbol{x}$ is rewritten as:

$$\boldsymbol{x} = \sum_{i=1}^{N} \alpha_i \boldsymbol{\psi}_i = \boldsymbol{\Psi\alpha} \tag{11}$$

where $\boldsymbol{\Psi}$ is the orthogonal basis matrix, which is composed of base vectors, $\boldsymbol{\alpha}$ is projection coefficient vector, and α_i is represented as $\alpha_i = \langle \boldsymbol{x}, \boldsymbol{\psi_i} \rangle$, namely, the inner product of signal and ith base vector.

Obviously, $\boldsymbol{x}$ and $\boldsymbol{\alpha}$ are equivalent representation of the same signal. $\boldsymbol{x}$ is time domain representation of the signal, and $\boldsymbol{\alpha}$ is the representation in orthogonal domain. When α_i has only K nonzero coefficient, namely $K \ll N$, signal $\boldsymbol{x}$ is called K-sparsity in certain orthogonal domain. In this case, Eq. (11) is the sparse representation of signal $\boldsymbol{x}$. According to CS theory, we can use observation matrix $\boldsymbol{\Phi} \in \boldsymbol{R}^{M\times N} (M \gg N)$ to conduct adaptively nonlinear transform of signal $\boldsymbol{x}$, which converts the signal $\boldsymbol{x}$ into observation vector $\boldsymbol{y} \in R^{M\times 1}$.

$$\boldsymbol{y} = \boldsymbol{\Phi x} \tag{12}$$

Substituting Eq. (11) into Eq. (12), the observation vector is rewritten as:

$$\boldsymbol{y} = \boldsymbol{\Phi x} = \boldsymbol{\Phi\Psi\alpha} = \boldsymbol{A\alpha} \tag{13}$$

where $\boldsymbol{A}$ is sensing matrix. Since the dimension M of the observation vector $\boldsymbol{y}$ is much smaller than the dimension N of the signal $\boldsymbol{x}$, we can achieve the purpose of signal compression.

If the signal contain the noise, the noisy signal can be represented as:

$$\boldsymbol{x}_n = \boldsymbol{x} + \boldsymbol{n}_w \tag{14}$$

where $\boldsymbol{x}$ is the original signal, and $\boldsymbol{n}_w$ is the noise.

The noisy observation matrix is calculated by substituting Eq. (14) into Eq. (13):

$$\boldsymbol{y}_n = \boldsymbol{\Phi}(\boldsymbol{x} + \boldsymbol{n}_w) = \boldsymbol{A}(\boldsymbol{\alpha} + \boldsymbol{\alpha}_n) \tag{15}$$

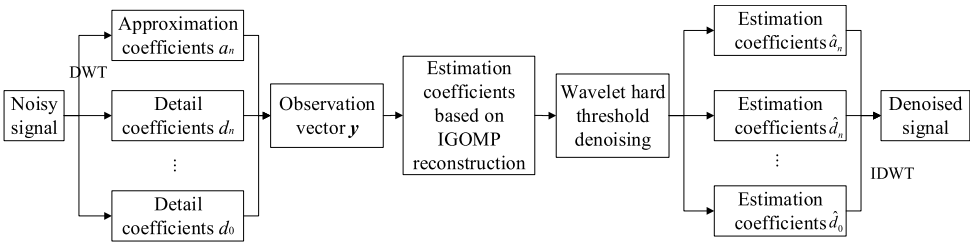

FIGURE 4. The diagram block of proposed algorithm.

where $\boldsymbol{\alpha}$ is the projection coefficient vector of original signal, and $\boldsymbol{\alpha}_n$ is the projection coefficient vector of noise.

According to the literature [32], compared the original signal, the noise in the $\boldsymbol{\Psi}$ domain is not sparse. In other words, the elements of vector $\boldsymbol{\alpha}_n$ are almost nonzero values. Thus, combing the sparse characteristics of original signal, we can retain K useful element to eliminate the noise component and recover signal by solving Eq. (15). The most direct reconstruction method is by solving Eq. (15) under l_0 norm:

$$\min \|\boldsymbol{\alpha}\|_0 \quad s.t. \quad \boldsymbol{A}\boldsymbol{\alpha} = \boldsymbol{y} \tag{16}$$

However, the inverse problem of solving Eq. (15) is an NP-Hard problem. Even if optimization problem is solved under l_1 norm, the enormous computation is unavoidable. many researchers have put forward reconstruction algorithm such as MP and OMP algorithm.

In conclusions, three key problems of CS denoising are signal decomposition, determination of K value and signal reconstructs algorithm.

With respect to the signal decomposition, we utilize discrete wavelet transform, discrete Fourier transform and discrete Cosine transform frequently. Owing to the signal feature and wavelet characteristics, noisy signal is decomposed using discrete wavelet base after the signal denoising based on improved SSA method. The diagram block of proposed algorithm is shown in Fig. 4.

We obtain the signal sequence $\boldsymbol{\alpha} = [a_n, d_n, d_{n-1} \ldots, d_o]^{\mathrm{T}}$ by using DWT. The output signal length through traditionally DWT is equal to input signal length plus filter response length minus one [44]. The total decomposition coefficient number of DWT is greater than that of original signal, which causes the additional component. To avoid redundant signal, output signal sequence are constructed with periodized extension method, followed by periodic convolution. Finally, principal values sequence is taken as the output signal sequence. The observation vector is calculated with a Gaussian measurement matrix by Eq. (15). Meanwhile, the original length is dramatically compressed. Compared with OMP algorithm, GOMP algorithm has better performance by rigorous proof [41], and the flow chart of GOMP algorithm is described as Fig. 5.

The GOMP algorithm needs to know the pre-knowledge of the K-sparsity, and inspired by singular value curvature spectrum, we propose the curvature analysis method to

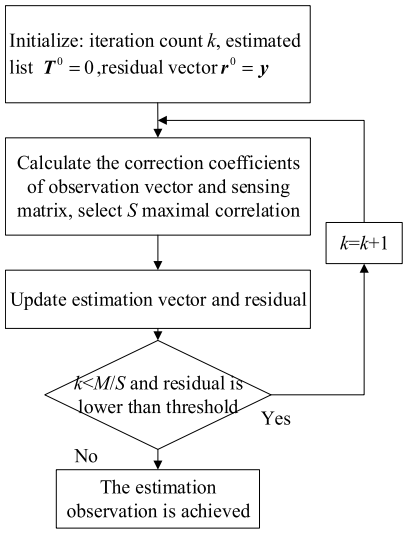

FIGURE 5. The flow chart of GOMP algorithm.

determine sparsity. The curvature function in discrete form is:

$$C(i) = \frac{|\boldsymbol{\alpha}(i+1) - 2\boldsymbol{\alpha}(i) + \boldsymbol{\alpha}(i-1)|}{(1 + (\boldsymbol{\alpha}(i) - \boldsymbol{\alpha}(i-1))^2)^{\frac{3}{2}}} \quad i = 1, \ldots, N-1 \tag{17}$$

The sparsity is determined using the identical method in Section 3. The peak points $C_{\mathrm{p}}(i)$ are searched by traversing all points. Find the minimum curvature point $C_{\mathrm{pmin}}(i)$ that is greater than the threshold, which is $\mathrm{mean}(C_{\mathrm{p}}) + q_2 \cdot \mathrm{std}(C_{\mathrm{p}})$. Meanwhile, in order to compromise between the accuracy and computation cost, we add correlation termination condition, which is expressed as $\mathrm{corr}(\boldsymbol{x}, \boldsymbol{\Psi}\hat{\boldsymbol{\alpha}}^k) > \mathrm{corr}(\boldsymbol{x}, \boldsymbol{\Psi}\hat{\alpha}^{k-1})$. Thus, the pseudocode of IGOMP algorithm is shown in Table 1. The whole process is as follows:

Step1: Initialize: iteration count $k = 0$, estimated list $T^0 = 0$, residual vector $\boldsymbol{r}^0 = \boldsymbol{y}$, and selection atom number S.

Step2: If the termination conditions, denoted as $\|\boldsymbol{r}^k\|_2 > \varepsilon$, $k < M/S$ and $\mathrm{corr}(\boldsymbol{x}, \boldsymbol{\Psi}\hat{\boldsymbol{\alpha}}^k) > \mathrm{corr}(\boldsymbol{x}, \boldsymbol{\Psi}\hat{\alpha}^{k-1})$, are satisfied, increment k and go to Step3. Otherwise, Go to Step5.

Step3: Calculate the inner product of observation vector and sensing matrix, and select S maximal values. Select atom columns Λ^k, which are corresponding to S maximal values. And then, update the estimated list $T^k = T^{k-1} \cup \Lambda^k$.

TABLE 1. The IGOMP algorithm.

Input: measurement matrix $\Phi \in R^{M\times N}$, observation vector $y \in R^{M}$, sparsity K, number of indices for each selection $S \pounds K$

Initialize: iteration count k=0, estimated list $T^0 = 0$, residual vector $r^0 = y$.

While $\|r^k\|_2 > \varepsilon$, $k < M/S$ and $\text{corr}(x, \Psi\hat{\alpha}^k) > \text{corr}(x, \Psi\hat{\alpha}^{k-1})$ do

$k = k + 1$.

$\Lambda^k = \arg\max_{\Lambda:|\Lambda|=s} \|(A^t r^{k-1})_\Lambda\|_1$.

$T^k = T^{k-1} \cup \Lambda^k$.

$\hat{\alpha}^k = \arg\min_{\text{supp}(u)=T^k} \|y - A\alpha\|_2$.

$r^k = y - A\hat{\alpha}^k$.

End

Output: the estimated support $\hat{T} \arg\min_{\Lambda:|\Lambda|=K} \|\hat{\alpha}^k - \hat{\alpha}^k_\Lambda\|_2$, signal $\hat{\alpha}$ satisfying $\hat{\alpha}_{\{1,\ldots,n\}\setminus\hat{T}} = 0$ and $\hat{\alpha}_{\hat{T}} = \Phi^+_{\hat{T}} y$.

Step4: Estimated signal sequence $\hat{\alpha}^k$ is calculated using least square method. Update the residual vector r^k. Go to Step 2.

Step5: Output estimated signal sequence $\hat{\alpha}$.

Despite the IGOMP algorithm can recover the elementary contour of original signal, the signal sometimes contains impulse noise on account of the wrong atoms. Moreover, arbitrary greedy algorithm reconstruct signal successfully with a certain probability. Thus, we adopt the hard threshold denoising method to remove the residual noise. In this paper, the hard threshold denoising aims at the detail coefficients, and hard threshold function is expressed as:

$$\beta = \begin{cases} 0, & |h| < T_h \\ h, & |h| \geq T_h \end{cases} \tag{18}$$

where h is the detail coefficient after IGOMP reconstruction algorithm, and T_h is the threshold, which is triple standard deviation of estimated noise level.

After updating the sequence, the inverse DWT is used to obtain completely denoised signal.

We select n as $N/2$, the computational complexity of ISSA algorithm is $O(N^3)$, and the computational complexity of IGOMP algorithm is $O(Klog(N/K))$. Therefore, the proposed computational complexity is $O(N^3)$, as N is big enough.

IV. SIMULATIONS

On account of the ranging requirement, we evaluate performance of signal denoising with two parameters: SNR, and peak time error (PTE).

SNR is defined as:

$$\text{SNR}=10\lg\frac{\|V(t)\|_2^2}{\left\|V(t)-\tilde{V}(t)\right\|_2^2} \tag{19}$$

where $V(t)$ is the original signal, and $\tilde{V}(t)$ is denoised signal.

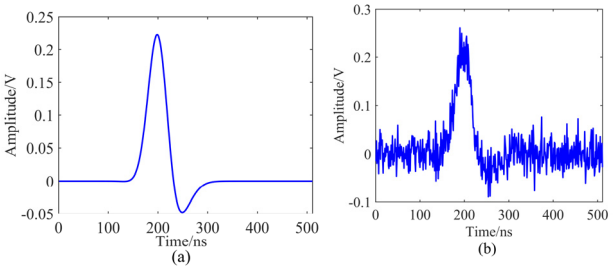

FIGURE 6. The simulation received laser signals: (a) original signal and (b) noisy signal with RMS noise voltage 25mV.

And PTE is:

$$\text{PTE} = \left|t_\text{p} - t_\text{d}\right| \tag{20}$$

where t_p is ideal time instant with respect to peak voltage, and t_d is time instant with respect to peak voltage after de-noising.

Assuming $A_1 = 0.3\text{V}, A_2 = -0.1\text{V}, A_3 = 0\text{V}, t_1 = 20\text{ns}, t_2 = 50\text{ns}, \tau_1 = 20\text{ns}, \tau_2 = 30\text{ns}, \overline{V}_n = 25\text{mV}$, time resolution to be 1ns, and the signal length N to be 512, simulation signals are shown in Fig. 6.

A. PROPOSED ALGORITHM

The paramters are: $q_1 = 0.1, q_2 = 0.1, S = 2, M/N = 0.4$. The wavelet decomposition level is 6, and the wavelet base is 'db4'. The row number n of data embedding is 256. The parameter r_2 is calculated as 0.8145. It can be seen from Figure 7 (a), the profile of singular value spectrum is complex. According to the proposed curvature spectrum, the threshold, marked as red line, is determined. Meanwhile, 19 singular values are retained. The denoised signal is depicted in Figure 7 (b). The partial noise is diminished. It provides the predenoising for CS denoising algorithm. The sparisity is 16 based on K-sparisity selection method. The denoised results are shown in Figure 7 (d). If we use IGOMP reconstruction algorithm without hard threshold, the denoised signal is incomplete. There would be remained impulse noise, which affects the ranging result. Therefore, the CS denoising method is not always efficient. In order to keep algorithm robust and efficient, the remained impulse noise shall be removed with wavelet hard threshold method. The threshold is based on the noise level of noisy signal. According to fifty sequences of noisy signal, the estimated noise level is 0.0239V, and T_h is 0.0711V. Fig. 7 (d) illustrates the recovered signal with hard threshold method (blue line), where the impulse noise is eliminated.

Finally, we compare the wavelet with soft threshold denoising, DFT with GOMP, and propose the algorithm. Comparing with other algorithms, the denoising curve of DFT with GMOP is not smooth due to the residual noise. On the other hand, it is unavailable to achieve the peak voltage or the corresponding time instant correctly. The ranging accuracy is severely limited, whatever the ranging method is used. The curve with soft threshold method is smoother than that of DFT with GMOP. However, partial useful signal

TABLE 2. SNRs with different algorithms.

Algorithm	SNR/dB with different equivalent RMS noise voltage/ mV					
	10	15	20	25	30	35
Hard threshold	19.8707	17.3019	14.8140	13.1319	11.3870	9.8035
Soft threshold	20.7493	19.4441	18.1912	17.1514	15.9958	14.2898
DFT with GOMP	22.4419	20.0384	17.4460	13.4644	9.9929	11.1464
DWT with IGOMP	20.7457	16.4021	14.3469	13.9407	11.7493	10.9975
ISSA+DFT with GOMP	22.4656	20.7289	16.6392	14.6803	13.0029	11.5780
ISSA+DFT with GOMP+smoothing filter	25.7390	23.9938	20.4671	18.2433	16.6196	15.4455
ISSA+ Hard threshold	23.8561	22.6331	20.4973	18.8588	17.3435	16.3250
ISSA+ Soft threshold	21.1426	20.6330	19.7623	18.6716	17.5749	16.7851
Proposed	**25.8439**	**23.4940**	**20.7780**	**20.4803**	**18.0995**	**17.6749**

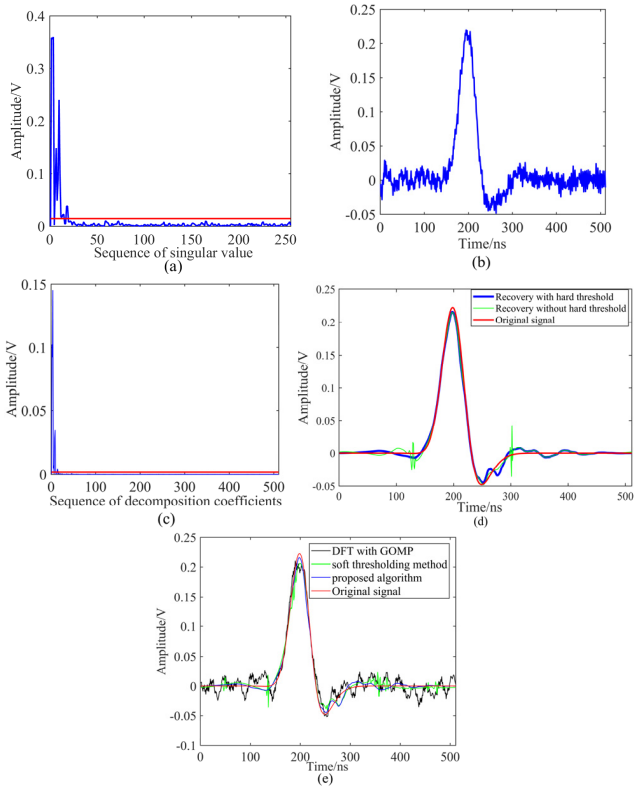

FIGURE 7. The denoised results. (a) Curvature spectrum with proposed threshold (red line). (b) The denoised signal after ISSA algorithm. (c) Curvature spectrum with wavelet decomposition results. (d) Denoised signal after two-stage denoising algorithm. (e) The denoised signal curves with different algorithms.

is lost. Even if peak time instant of DFT with GMOP is similar to that of the original signal, the peak voltage will be lower than original one. The proposed algorithm could correct this deficiency. The CS with IGMOP prevents the peak voltage decrease. Moreover, the peak inverse voltage is the same as original voltage. It can keep point cloud more precisely for laser radar.

B. ALGORITHM COMPARISION

To compare denoised efficiency, we calculate SNR of different algorithms with different RMS noise voltage. The algorithms adopted are: hard threshold, soft threshold, DFT with GOMP, DWT with GOMP, ISSA + DFT with GOMP, ISSA + DFT with GOMP + smoothing filter, ISSA + Hard threshold, ISSA + Soft threshold and proposed algorithms. The paramters are: $q_1 = 0.1$, $q_2 = 0.1$, $S = 2$, $M/N = 0.4$. The wavelet decomposition level is 6, and the wavelet base is 'db4'. SNRs and PTEs with different algorithms are shown in Table 2 and 3 respectively. As can be seen from Table 2, SNR of the proposed algorithm is the best. Meanwhile, SNR of hard threshold is the worst. Whilst equivalent RMS noise voltage is 10mV, SNRs of DFT with GOMP and DWT with IGOMP are higher than those of soft threshold and hard threshold method. Nevertheless, the situation is opposite with lower SNRs. It means that denoised performance based on CS theory with GOMP is limited in low SNRs. After denoising with the proposed ISSA algorithm, SNRs of soft threshold and hard threshold methods are remarkably improved. Additional, SNRs of the two improved threshold methods tend to be consistent with the decrease of noise voltage. However, SNR of DFT with GOMP after denoising signal with ISSA increases slightly. Because the signal is not smooth as indicated in Fig. 7 (e), we improve SNR with smoothing filter. Although SNR is increased by more than 3dB with different noise using smoothing filter, this algorithm is no better than the proposed algorithm either. In addition to SNR, we focus on PTE based on ranging principle. It can been see from Table 3 that the PTEs of proposed algorithm with different noise are zeros with time resolution of 1ns. Moreover, the PTEs of hard threshold, soft threshold, DFT with GOMP and DWT with GOMP through proposed ISSA are on a downward trend. The PTEs of hard threshold, soft threshold methods with proposed ISSA reduce to 1ns. Two-stage noise algorithm can improve the ranging accuracy and reduce the noise.

C. INFLUENCE OF DIFFERENT PARAMETERS

1) the PARAMETER OF issa ALGORITHM

We have denotated θ_T as $\text{mean}(\sigma_k)+q_1 \cdot \text{std}(\sigma_k)$ in Section III. The θ_T is determined by parameter q_1, and it is crucial to decide the value of parameter q_1. SNRs of proposed algorithm with different q_1 are calculated and shown in Table 4. When q_1 is positive between 0 and 1, SNRs of different equivalent RMS noise voltage are almost invariable. While the q_1 is 0 and the noise voltages are 30mV and 35mV, SNRs are lower

TABLE 3. PTEs with different algorithms.

Algorithm	PTE/ns with different equivalent RMS noise voltage/ mV					
	10	15	20	25	30	35
Hard threshold	8	1	8	8	8	8
Soft threshold	2	1	1	2	2	3
DFT with GOMP	1	1	4	4	1	4
DWT with IGOMP	1	2	8	6	6	7
ISSA+DFT with GOMP	1	1	3	1	6	6
ISSA+DFT with GOMP+smoothing filter	1	1	3	3	3	3
ISSA+ Hard threshold	1	0	1	1	1	0
ISSA+ Soft threshold	1	0	1	1	1	0
Proposed	**0**	**0**	**0**	**0**	**0**	**0**

TABLE 4. SNRs of proposed algorithm with different q_1.

q_1	SNR/dB with different equivalent RMS noise voltage/ mV					
	10	15	20	25	30	35
-1	20.7462	16.4038	14.3480	13.9415	11.7497	10.9981
-0.8	20.7462	16.4038	14.3480	13.9415	11.7497	10.9981
-0.6	20.7462	16.4038	14.3480	13.9415	11.7497	10.9981
-0.4	20.7462	16.4038	14.3480	13.9415	11.7497	10.9981
-0.2	20.7462	16.4038	14.3480	13.9415	11.7497	10.9981
0	25.8439	22.8284	20.7780	20.4803	11.8199	11.0670
0.2	25.7585	21.6319	20.7780	20.4803	18.0995	17.6749
0.4	25.7585	21.6319	21.0470	20.4803	18.0995	17.6749
0.6	25.7585	21.6319	21.0470	20.4803	18.0995	17.6749
0.8	25.7585	21.6319	21.0470	20.3785	18.0590	17.5801
1	25.7585	21.6319	21.0470	20.3785	18.0590	17.5801

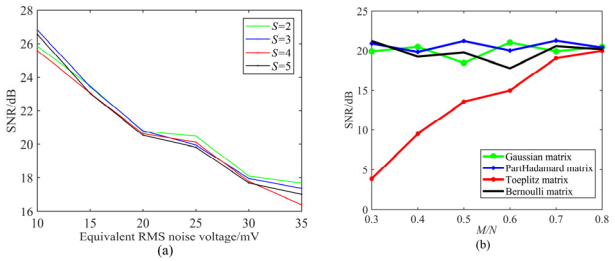

FIGURE 8. The influences of different parameters on denoised results. (a) Different number of indices S. (b) Different observation matrices and the dimension M.

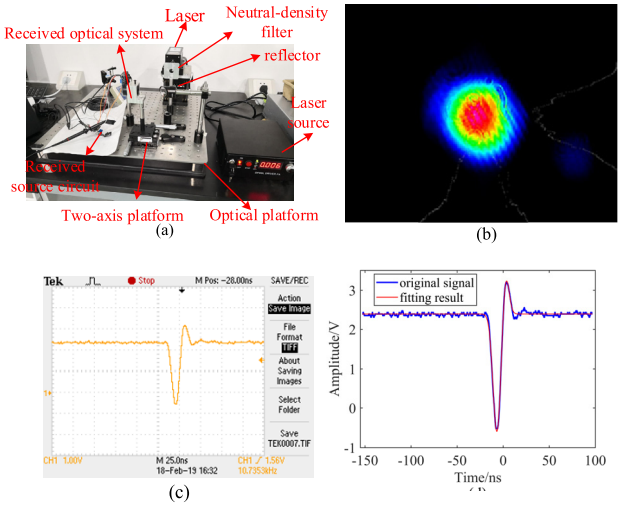

FIGURE 9. Experiments setup and results. (a) The experiments setup. (b) laser beam distribution. (c) Laser received waveform at 5m. (d) Fitting curve of received signal.

than those of positive q_1. Specifically, as the scope of q_1 is from -1 to 0, r_1 is 1. It means that the first stage denoising method is not efficient. Thus, when the noise voltage is higher than 15mV, the q_1, selected as 0.1, is the best for ISSA algorithm. In higher SNR situation, the q_1 should be selected to be close to 0.

2) THE PARAMETERS OF IGOMP ALGORITHM

In addition to the parameters of ISSA, The number of indices S, observation matrix and dimension M of IGOMP algorithm affect the denoising results as well. Hence, the influences of different parameters on denoised results are furthermore studied. Assuming that the other parameters are the same as part A. Fig. 8 (a) illustrates SNRs of different parameters S with different equivalent RMS noise voltages. While different equivalent RMS noise voltage increases, SNR decreases. However, it is not in accordance with the parameter S. When the noise voltage is between 15mV and 35mV, SNR is highest with $S = 2$. As the noise is 10mV, SNR of $S = 2$ is lower than that of $S = 3$ or $S = 5$ with 10mV. Generally, SNR is superior with $S = 2$. From Fig. 8 (a), SNR is less influenced by parameter S.

Supposing that the other parameters are the same as part A. SNRs of different observation matrices and the dimension M are shown in Fig. 8 (b). We calculated SNRs of Gaussian matrix, partial Hadamard matrix, Toeplitz matrix and Bernoulli matrix, respectively. Although the compression ratio M/N increases, SNRs corresponding to Gaussian matrix, partial Hadamard matrix and Bernoulli matrix fluctuate around 20dB. The change regulation of partial Hadamard matrix and Bernoulli matrix is identical. The rate of change respect to Gaussian matrix are opposite to the three matrices mentioned above. While M/N is 0.6, SNR is largest for Gaussian matrix. But the computational cost rises in the meantime. After balancing between SNR and computational cost, it is the most suitable for denoising processing by using compression ratio 0.4. It is worth noting that SNRs corresponding to Toeplitz matrix are special. The larger the compression ratio M/N is, the bigger SNR is. Nevertheless, whatever the compression ratio, SNRs of Gaussian matrix, partial Hadamard matrix and Bernoulli matrix are higher

TABLE 5. Parameters of laser.

Parameters	Value
Threshold current	3 A
Rated operational current	7 A
Single pulse energy	40μJ
Pulse width	15ns
waist radius	1.3mm
beam divergence angle	0.8mrad

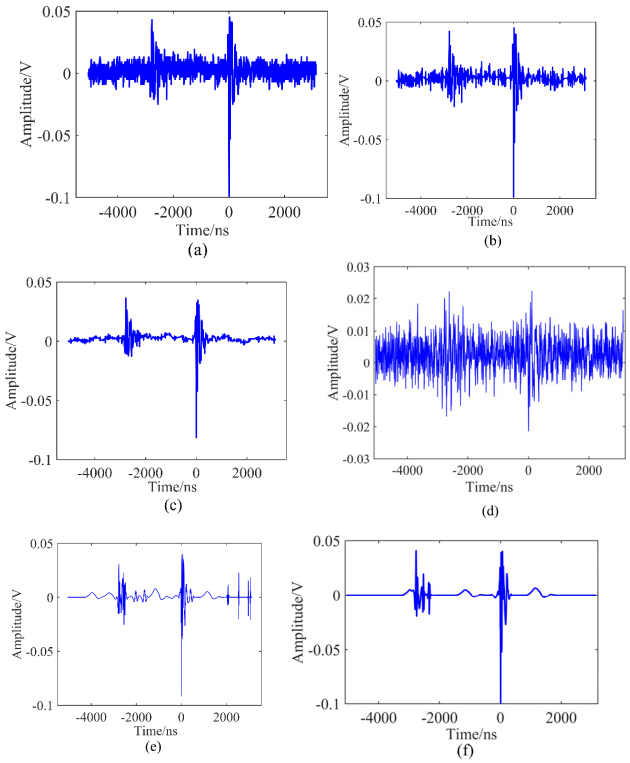

FIGURE 10. Denoised results. (a) The original received waveform. (b) Denoised signal with hard threshold method. (c) denoised signal with soft threshold method. (d) Denoised signal based on DFT with GOMP algorithm. (e) Denoised signal based on DWT with GOMP algorithm. (f) Denoised signal based on proposed algorithm.

than those of Toeplitz matrix. In summary, Gaussian matrix, partial Hadamard matrix and Bernoulli matrix are appropriate for IGOMP algorithm.

V. EXPERIMENTAL

The experiments setup is shown in Fig. 9 (a). The light source is 1064nm pulse diode-pumped solid-state laser. The laser parameters are listed in Table 5. The beam divergence angle is 0.8mrad. This small divergence angle is beneficial for laser radar system. The laser beam, as shown in Fig. 9 (b), exhibits Gaussian distribution. It is therefore substantial for received signal measurement experiment. Although the laser power is adjustable, it is too high to conduct experiments. Therefore, neutral-density filter with attenuation rate 40% is used to control the laser power. The radius of neutral-density filter is

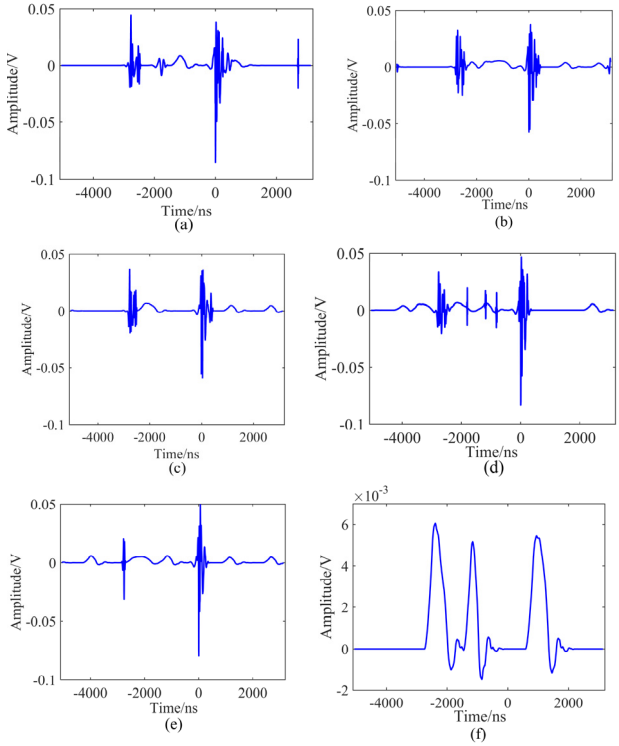

FIGURE 11. Denoised results of proposed algorithm with different parameters. (a) $q_1 = -0.1$. (b) $q_1 = 0.1$. (b) $S = 2$. (c) $S = 4$. (e) $T_h = 0.05$V. (f) $T_h = 0.1$V.

15mm. A 45-degree reflector is mounted on optical platform. The received optical system is mounted on two-axis platform to adjust light path, and the resolution is 10μm. The type of oscillograph is TBS1104. The sampling rate is 1GHz, and bandwidth is 100MHz. When target, as diffusion reflector, is placed at 5m away from laser radar, the original voltage signal is shown in Fig.9 (c). We fit the curve for received signal. The fitting results are: $A_1 = -3.027$V, $A_2 = 1.046$V, $A_3 = 2.446$V, $t_1 = 6.12$ns, $t_2 = 5.071$ns, $\tau_1 = -6.767$ns, $\tau_2 = 2.653$ns, $A_3 = 2.4$V.

In order to compare denoised effect, another measurement experiment was carried out. The distance between target and laser radar is 5m. Original waveform is shown in Fig. 10 (a), and maximum value is approximately 100mV at 0ns. On account of electromagnetic radiation interference of power supply, coupled noise, as an impulse noise, is mixed with receiving signal. The signal length is 2048. The paramters of denoised signal are set as: $q_1 = 0.01$, $S = 3$, $M/N = 0.5$. $q_2 = 0.1$, $T_h = 0.0129$V. The wavelet decomposition level is 6, and the wavelet base is 'db4'. The demonised result retain the peak of signal with wavelet hard threshold method, but the noise still exists. Although the noise removed with wavelet soft threshold method, the signal amplitude diminishes as well. Rather than removing noise, the DFT with GOMP algorithm distorts signal furthermore. The denoised effect of DWT with GOMP algorithm is better than that of wavelet soft threshold method. However, there are partial spike noises mixed in signal. Comparing with

above algorithms, proposed algorithm shows outstanding performance. The partial spike noise is removed, yet the peak voltage does not attenuate.

In order to analyze denoised results of different parameters, the denoised experiments of proposed algorithm with different parameters are carried out and shown in Fig. 11. The parameters are the same as mentioned above. The denoised signal of Fig. 11 (a) is similar to that of Fig. 10 (e). According to the simulation results, in this situation, the first-stage denoising method is disabled, and the spike noise exists. When q_1 is 0.1, the noise and peak value diminish simultaneously. The peak value is about -0.05mV, and the denoising performance is not the best. Combined with the simulations, due to 4.3mV noise level, the best q_1 should be lower than 0.1. From Fig. 11 (c) and (d), it is tough to select parameter S, which should be adjusted in experimentally. Finally, from Fig. 11 (e) and (f), if the threshold is larger than recommended value, the signal reduces to certain extent. The larger the threshold is, the smaller the peak value would be.

VI. CONCLUSION

The principle of laser radar is introduced, and the received signal model is described. The cut-off point among singular values is determined by SSA algorithm fused with singular value selection method. Furthermore, the CS denoising algorithm based on improved GOMP reconstruction algorithm with hard threshold denoising method enhances SNR. SNR and peak time error calculation are conducted to evaluate denoised effect among different algorithms. The experimental setup is built up, and the de-noising experiments are carried out.

Some conclusions are achieved: (1) The proposed ISSA algorithm can keep the useful signal and cut down the noise. In addition, after using ISSA algorithms, the performances of other denoised algorithms are of varying degrees improvement through simulations. (2) CS denoising algorithm based on IGOMP with hard threshold denoising method eliminates the spike noise. Meanwhile, the failure probability of IGOMP is smaller than that of OMP. (3) Compared with other algorithms, the proposed algorithms performance is the best.

Our future work focus on full-waveform ranging accuracy based on the proposed algorithm, especially in multi-target ranging applications. Since the laser beam irradiates on multi targets and the partial scattered light from target at long range is weak, the proposed algorithm is suits well for this situation.

REFERENCES

[1] B. Schwarz, "LIDAR: Mapping the world in 3D," *Nature Photon.*, vol. 4, pp. 429–430, Jul. 2010.

[2] I. Ashraf, S. Hur, and Y. Park, "An investigation of interpolation techniques to generate 2D intensity image from LIDAR data," *IEEE Access*, vol. 5, pp. 8250–8260, 2017.

[3] E. Javanmardi, M. Javanmardi, Y. Gu, and S. Kamijo, "Factors to evaluate capability of map for vehicle localization," *IEEE Access*, vol. 6, pp. 49850–49867, 2018.

[4] Y. Cheng, J. Cao, Q. Hao, Y. Xiao, F. Zhang, W. Xia, K. Zhang, and H. Yu, "A novel de-noising method for improving the performance of full-waveform LiDAR using differential optical path ," *Remote Sens.*, vol. 9, no. 11, p. 1109, Oct. 2017.

[5] S. Nie, C. Wang, X. Xi, G. Li, S. Luo, X. Yang, P. Wang, X. Xi, G. Li, S. Luo, X. Yang, P. Wang, and X. Zhu, "Exploring the influence of various factors on slope estimation using large-footprint LiDAR data," *IEEE Trans. Geosci. Remote Sens.*, vol. 56, no. 11, pp. 6611–6621, Nov. 2018.

[6] S. Budzan and J. Kasprzyk, "Fusion of 3D laser scanner and depth images for obstacle recognition in mobile applications," *Opt. Lasers Eng.*, vol. 77, pp. 230–240, Feb. 2016.

[7] X. Xu, M. Luo, Z. Tan, M. Zhang, and H. Yang, "Plane segmentation and fitting method of point clouds based on improved density clustering algorithm for laser radar," *Infr. Phys. Technol.*, vol. 96, pp. 133–140, Jan. 2019.

[8] J. Haijiao, J. Lai, Y. Wei, W. Chunyong, and L. Zhenhua, "Theoretical distribution of range data obtained by laser radar and its applications," *Opt. Laser Technol.*, vol. 45, pp. 278–284, Feb. 2013.

[9] S. Johnson and S. Cain, "Bound on range precision for shot-noise limited ladar systems," *Appl. opt.*, vol. 47, no. 28, pp. 5147–5154, Oct. 2008.

[10] L. Jiancheng, J. Haijiao, Y. Wei, W. Chunyong, and L. Zhenhua, "Range uncertainty distribution of direct-detection laser radar with a peak-detecting routine," *Optik*, vol. 124, no. 21, pp. 5202–5205, Nov. 2013.

[11] X. Li, B. Yang, X. Xie, D. Li, and L. Xu, "Influence of waveform characteristics on LiDAR ranging accuracy and precision," *Sensors*, vol. 18, no. 4, p. 1156, 2018.

[12] G. Carter, C. Knapp, and A. Nuttall, "Estimation of the magnitude-squared coherence function via overlapped fast Fourier transform processing," *IEEE Trans. Audio Electroacoust.*, vol. 21, no. 4, pp. 337–344, Aug. 1973.

[13] X. Ouyang and M. G. Amin, "Short-time Fourier transform receiver for nonstationary interference excision in direct sequence spread spectrum communications," *IEEE Trans. Signal Process.*, vol. 49, no. 4, pp. 851–863, Apr. 2001.

[14] P. Chai, X. Luo, and Z. Zhang, "Image fusion using quaternion wavelet transform and multiple features," *IEEE Access*, vol. 5, pp. 6724–6734, 2017.

[15] Z. Zhou, D. Hua, Y. Wang, Q. Yan, S. Li, Y. Li, and H. Wang, "Improvement of the signal to noise ratio of Lidar echo signal based on wavelet de-noising technique," *Opt. Lasers Eng.*, vol. 51, no. 8, pp. 961–966, Aug. 2013.

[16] M. Srivastava, C. L. Anderson, and J. H. Freed, "A new wavelet denoising method for selecting decomposition levels and noise thresholds," *IEEE Access*, vol. 4, pp. 3862–3877, 2016.

[17] N. E. Huang, Z. Shen, S. R. Long, M. C. Wu, H. H. Shih, Q. Zheng, N.-C. Yen, C. C. Tung, and H. H. Liu, "The empirical mode decomposition and the Hilbert spectrum for nonlinear and non-stationary time series analysis," *Proc. Roy. Soc. London, Ser. A, Math., Phys. Eng. Sci.*, vol. 454, no. 1971, pp. 903–995, Mar. 1998.

[18] J. Su, Y. Wang, X. Yang, and X. Wang, "Enhancement of weak lidar signal based on variable frequency resolution EMD," *IEEE Photon. Technol. Lett.*, vol. 28, no. 24, pp. 2882–2885, Dec. 15, 2016.

[19] N. Golyandina and A. Zhigljavsky, *Singular Spectrum Analysis for Time Series*. Berlin, Germany: Springer, 2013.

[20] X. Li and Y. Huang, "Lidar signal de-noising based on discrete wavelet transform," *Chin. Opt. Lett.*, vol. 5, no. S1, pp. S260–S263, May 2007.

[21] M. Nasri and H. Nezamabadi-Pour, "Image denoising in the wavelet domain using a new adaptive thresholding function," *Neurocomputing*, vol. 72, nos. 4–6, pp. 1012–1025, Jan. 2009.

[22] X. Chen, G. Cheng, H. Li, and Y. Li, "Fault identification method for planetary gear based on DT-CWT threshold denoising and LE," *J. Mech. Sci. Technol.*, vol. 31, no. 3, pp. 1035–1047, Mar. 2017.

[23] D. L. Donoho, "De-noising by soft-thresholding," *IEEE Trans. Inf. Theory*, vol. 41, no. 3, pp. 613–627, May 1995.

[24] X.-P. Zhang, "Thresholding neural network for adaptive noise reduction," *IEEE Trans. Neural Netw.*, vol. 12, no. 3, pp. 567–584, May 2001.

[25] H. Liu, W. Wang, C. Xiang, L. Han, and H. Nie, "A de-noising method using the improved wavelet threshold function based on noise variance estimation," *Mech. Syst. Signal Process.*, vol. 99, pp. 30–46, Jan. 2018.

[26] X. Wang, X. Ou, and B.-W. Chen, "Image denoising based on improved wavelet threshold function for wireless camera networks and transmissions," *Int. J. Distrib. Sensor Netw.*, vol. 11, no. 9, Sep. 2015, Art. no. 670216.

[27] P. Flandrin, G. Rilling, and P. Goncalves, "Empirical mode decomposition as a filter bank," *IEEE Signal Process. Lett.*, vol. 11, no. 2, pp. 112–114, Feb. 2004.

[28] J. Chang, L. Zhu, H. Li, F. Xu, B. Liu, and Z. Yang, "Noise reduction in Lidar signal using correlation-based EMD combined with soft thresholding and roughness penalty," *Opt. Commun.*, vol. 407, pp. 290–295, Jan. 2018.

[29] X. Zhao and B. Ye, "Selection of effective singular values using difference spectrum and its application to fault diagnosis of headstock," *Mech. Syst. Signal Process.*, vol. 25, no. 5, pp. 1617–1631, Jul. 2011.
[30] X.-Z. Zhao, B.-Y. Ye, and T.-J. Chen, "Selection of effective singular values based on curvature spectrum of singular values," *J. South China Univ. Technol.*, vol. 38, no. 6, pp. 11–18, Jun. 2010.
[31] W.-X. Yang and P. W. Tse, "Development of an advanced noise reduction method for vibration analysis based on singular value decomposition," *NDT E Int.*, vol. 36, no. 6, pp. 419–432, Sep. 2003.
[32] D. L. Donoho, "Compressed sensing," *IEEE Trans. Inf. Theory*, vol. 52, no. 4, pp. 1289–1306, Apr. 2006.
[33] M. F. Duarte and Y. C. Eldar, "Structured compressed sensing: From theory to applications," *IEEE Trans. Signal Process.*, vol. 59, no. 9, pp. 4053–4085, Sep. 2011.
[34] Y. Chen, Z. Liu, and H. Liu, "A method of fiber Bragg grating sensing signal de-noise based on compressive sensing," *IEEE Access*, vol. 6, pp. 28318–28327, 2018.
[35] S. Qu, J. Chang, Z. Cong, H. Chen, and Z. Qin, "Data compression and SNR enhancement with compressive sensing method in phase-sensitive OTDR," *Opt. Commun.*, vol. 433, pp. 97–103, Feb. 2019.
[36] M.-F. Zhao, P. Tang, B. Tang, P. He, Y.-F. Xu, S.-X. Deng, and S.-H. Shi, "Research on denoising of UV-Vis spectral data for water quality detection with compressed sensing theory based on wavelet transform," *Spectrosc. Spectral Anal.*, vol. 38, no. 3, pp. 844–850, Mar. 2018.
[37] J. A. Tropp and A. C. Gilbert, "Signal recovery from random measurements via orthogonal matching pursuit," *IEEE Trans. Inf. Theory*, vol. 53, no. 12, pp. 4655–4666, Jan. 2007.
[38] D. Needell and R. Vershynin, "Signal recovery from incomplete and inaccurate measurements via regularized orthogonal matching pursuit," *IEEE J. Sel. Topics Signal Process.*, vol. 4, no. 2, pp. 310–316, Apr. 2010.
[39] D. Needell and J. A. Tropp, "CoSaMP: Iterative signal recovery from incomplete and inaccurate samples," *Appl. Comput. Harmon. Anal.*, vol. 26, no. 3, pp. 301–321, May 2009.
[40] W. Dai and O. Milenkovic, "Subspace pursuit for compressive sensing signal reconstruction," *IEEE Trans. Inf. Theory*, vol. 55, no. 5, pp. 2230–2249, May 2009.
[41] J. Wang, S. Kwon, and B. Shim, "Generalized orthogonal matching pursuit," *IEEE Trans. Signal Process.*, vol. 60, no. 12, pp. 6202–6216, Dec. 2012.
[42] D. L. Donoho, Y. Tsaig, I. Drori, and J. Starck, "Sparse solution of underdetermined systems of linear equations by stagewise orthogonal matching pursuit," *IEEE Trans. Inf. Theory*, vol. 58, no. 2, pp. 1094–1121, Feb. 2012.
[43] T. Blumensath and M. E. Davies, "Stagewise weak gradient pursuits," *IEEE Trans. Signal Process.*, vol. 57, no. 11, pp. 4333–4346, Nov. 2009.
[44] L. H. Sun, Z. Yang, and L. Ye, "Speech compression and reconstruction based on adaptive multiscale compressed sensing theory," *Acta Electron. Sinica*, vol. 39, no. 1, pp. 40–45, Jan. 2011.

XIAOBIN XU received the B.E. and Ph.D. degrees from the Nanjing University of Science and Technology, China, in 2012 and 2017, respectively. He is currently a Lecturer with Hohai University. His current research interests include optical imaging, point cloud processing, and signal processing.

MIN ZHANG is currently pursuing the M.E degree with the College of Mechanical and Electrical Engineering, Hohai University, China. Her research interests include signal processing, SLAM, and 3D reconstruction.

MINZHOU LUO received the D.S. degree in control science and engineering from the University of Science and Technology of China, Hefei, China. He is currently a Professor with Hohai University. His research interests include bionics, service and industrial robots, and industry 4.0 technology.

JIAN YANG received the B.S. and Ph.D. degrees from the School of Mechanical Engineering, Nanjing University of Science and Technology, in 2005 and 2016, respectively. He is currently a Lecturer with the College of Mechanical Engineering, Yangzhou University. His current research interests include signal processing, neural networks, and compressed sensing.

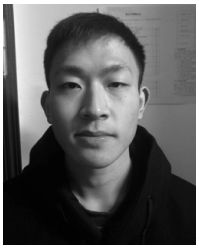

QINYANG QU is currently pursuing the bachelor's degree with Hohai University, China. His research interests include mechanical design, circuit design, and microcontroller programming.

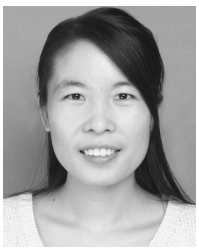

ZHIYING TAN received the Ph.D. degree in computer software and theory from the University of Electronic Science and Technology of China, in 2013. She is currently a Lecturer with Hohai University. Her major research interests include numerical analysis, image processing, and machine vision.

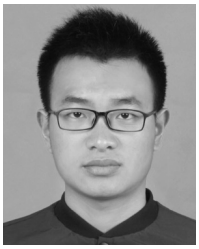

HAO YANG is currently pursuing the M.E. degree with Hohai University, China. His research interests include mobile robot and motor control.